International Journal of Fracture 24 (1984) 209–228

Local stress and strain fields near a spherical elastic inclusion in a plastically deforming matrix

R.D. THOMSON and J.W. HANCOCK

James Watt Engineering Laboratories, University of Glasgow, Scotland, UK

(Received June 5, 1983)

Abstract

At a micro-scale, fracture often starts in the vicinity of inclusions in a deforming matrix where the local stress and strain conditions may lead to either failure of the inclusion/matrix interface or of the particle itself. Analytic solutions are available for the local stress and strain fields near an elastic inclusion in an elastically deforming matrix but for plastic deformation it is necessary to resort to numerical analyses. Here a numerical solution is presented for a spherical elastic inclusion in an elastic/plastic matrix, concentrating largely on the particle/matrix interface which is of relevance to ductile fracture. Solutions are also presented for rigid and elastic inclusions in hardening and non-hardening matrices.

Nomenclature

Basic symbols	*Meaning*
E	uniaxial elastic modulus
e	strain
k	yield stress in shear
n	power hardening index
y	principal loading direction
α	1st slip direction in plane strain
β	2nd slip direction in plane strain
σ	normal stress
τ	shear stress

Superscripts	*Meaning*
el	elastic component
p	plastic component
– (overbar)	effective, representative or equivalent value

Subscripts	*Meaning*
0	initial yield value in uniaxial tension
max	maximum value
yy	component in loading direction
rr	component in radial direction
$\theta\theta$	component in 1st spherical direction
$\phi\phi$	component in 2nd spherical direction
∞	remote value of variable

1. Elastic solutions

The general problem of the elastic stress and strain fields for ellipsoidal elastic inclusions has been solved by Eshelby [1] who found that the fields within the inclusion are homogeneous. Although solutions for spherical and cylindrical inclusions may be derived

as special cases of Eshelby's analysis, it is often more convenient to refer to earlier work by Goodier [2]. In this, the solution for uniaxial tension is expressed in terms of arbitrary constants which are adjusted such that the appropriate boundary conditions are met on a closed path equivalent to the interface of the inclusion. The boundary condition for a rigid inclusion gives vanishing resultant displacements on the interface, while vanishing resultant stresses give the condition for a void. Goodier's [2] results show that the maximum radial stress on the interface of a cylindrical inclusion under a remote uniaxial tensile stress σ_∞ occurs in the loading direction and has a magnitude

$$\sigma_{rr\,\max} = 1.5\sigma_\infty.$$

The solution for a general multiaxial loading can be obtained from the uniaxial solution by superposition. The elastic stress field for a remote pure shear τ_∞ is then found by adding the stress field for a uniaxial tension of magnitude $+\tau_\infty$ to that for a uniaxial tension of magnitude $-\tau_\infty$ rotated through an angle of $\omega = \pi/2$ from the $+\tau_\infty$ direction (Fig. 1). The maximum value of the interfacial radial stress for a rigid cylindrical inclusion under pure shear loading then becomes

$$\sigma_{rr\,\max} = 2\tau_\infty$$

at $\omega = 0$, at which point the shear stress is zero and σ_{rr} is a principal stress. The remote principal stresses for an incompressible material in plane strain and subject to pure shear are

$$\sigma_{1\infty} = \tau_\infty \quad \sigma_{2\infty} = -\tau_\infty \quad \sigma_{3\infty} = 0.$$

The relation between the shear stress τ and the effective stress $\bar{\sigma}$

$$\bar{\sigma} = \tau\sqrt{3},$$

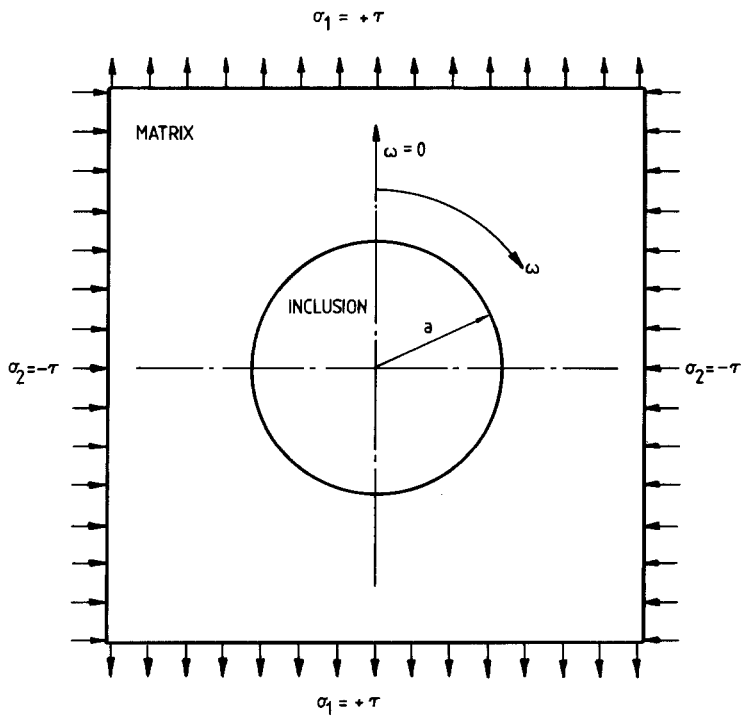

Figure 1. Cylindrical inclusion.

allows the maximum interfacial radial stress to be written as

$$\sigma_{rr\,\max} = (2/\sqrt{3})\,\bar{\sigma}_\infty.$$

Since the principle of superposition is valid for linear elastic materials, the stress field for any remote plane strain triaxial loading may be obtained by summing a remote pure shear field and a remote stress field with the appropriate hydrostatic component $\sigma_{m\infty}$ to give

$$\sigma_{rr\,\max} = 1.15\bar{\sigma}_\infty + \sigma_{m\infty}.$$

For a rigid spherical inclusion in uniaxial tension, Goodier [2] found that

$$\sigma_{rr\,\max} = 2\sigma_\infty$$

due to a remote uniaxial stress σ_∞ which can also be generalised to any axisymmetric loading by superimposing an appropriate hydrostatic stress to give:

$$\sigma_{rr\,\max} = 1.67\bar{\sigma}_\infty + \sigma_{m\infty}.$$

2. Elastoplastic solutions for cylindrical inclusions

The problem of a cylindrical elastic inclusion in both hardening and nonhardening elastic/plastic matrices was addressed by Orr and Brown [3]. Plane strain finite difference solutions for different biaxial loadings indicated that the stress distribution around the interface for triaxial loading was the sum of the stresses due to the pure shear component and the hydrostatic or mean component. While superposition may not be rigorously applied to elastic/plastic problems, this numerical result is of considerable practical use. In all the solutions, the maximum interfacial stress occurred at about $\pi/8$ from the direction of the remote maximum principal stress. If the initial yield stress in uniaxial tension is defined as σ_0 then for remote plastic strains of the order of 15 times the remote initial yield strain, the distribution of the radial stress around the inclusion took the approximate form

$$\sigma_{rr} = 1.75\sigma_0 \sin 4\omega + \sigma_{m\infty} \quad \pi/24 < \omega < 11\pi/24$$

in the non-hardening case and

$$\sigma_{rr} = 2.10\sigma_0 \sin 4\omega + \sigma_{m\infty} \quad \pi/24 < \omega < 11\pi/24$$

in the hardening case. Interestingly, despite significant plastic strains the solution of Orr and Brown [3] did not reach a steady state and while indicating the location and instantaneous value of the maximum interfacial radial stress, these expressions are not applicable throughout the loading history.

A useful feature of the Orr and Brown [3] solution is their plot of the directions of maximum shear strain around the inclusion from which the form of a possible slip-line field may be inferred (Fig. 2). For pure shear, the slip-lines remote from the inclusion are at an angle $\omega = \pi/4$ to the greatest principal stress and the symmetry of the problem implies that the slip-lines meeting the inclusion at multiples of $\pi/4$ must remain straight until they meet the interface. The α-line which meets the inclusion at $\pi/4$ in Fig. 2 must be straight and it follows that the local mean stress on the interface is the same as the mean stress in the remote field. Since the remote mean stress is zero in pure shear, then

$$\sigma_m = \sigma_{m\infty} = 0 \quad \text{at} \quad \omega = \pi/4.$$

For a plastically deforming matrix adjacent to a rigid inclusion the α-slip-lines must meet the interface radially and the β-slip-lines tangentially. The β-line tangential to the interface must cross the remote tensile axis ($\omega = 0$) at $\pi/4$ if it is to be orthogonal to the α-line from the other side of the axis. The β-line must therefore break away from the

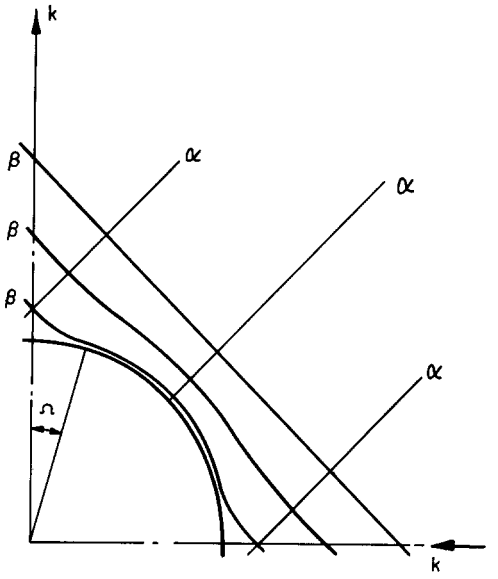

Figure 2. Form of a slip-line field around a cylindrical inclusion.

interface at some angle $\omega = \Omega$ which is indeterminate at present but has limiting values $\Omega = 0$ and $\Omega = \pi/4$. Application of the Hencky equations gives the maximum possible radial stress around the interface in terms of the remote yield stress k in shear as

$$\sigma_{rr} = 2k(\pi/4 - \Omega).$$

If the case of $\Omega = \pi/4$, all but the point on the interface at $\pi/4$ is rigid and the straight slip-lines form a square which circumscribes the inclusion. In the case when Ω approaches 0, the maximum possible interfacial radial stress approaches $0.5\pi k$ which with

$$\sigma_0 = \sqrt{3}\,k,$$

$$\Rightarrow \sigma_{rr\,\max} = 0.9\sigma_0$$

in the direction of the maximum principal stress ($\omega = 0$). This limiting case of $\Omega = 0$ will give an upper limit on the interfacial stress concentration. Superposition of a hydrostatic stress does not change the nature of the slip-line field for an incompressible material and leads finally to an expression of the form

$$\sigma_{rr\,\max} = 0.9\sigma_0 + \sigma_{m\infty}.$$

Argon, Im and Safoglu [4] modelled the inclusion problem in plane strain as a rigid cylinder embedded in a finite element mesh of triangular elements. The stress and strain fields in the matrix were evaluated for an applied shear loading using the elastic/plastic finite element program of Marcal and King [5]. The analysis was performed for a linear-elastic/perfectly-plastic matrix up to remote strains of the order of the elastic yield strain when the interfacial radial stress is given approximately by

$$\sigma_{rr} = 1.5k \cos 2\omega.$$

This implies a maximum value $\sigma_{rr\,\max}$ of $1.5k$, in accord with the $(\pi/2)k$ for the limiting value of the slip-line field. In contrast with the work of Orr and Brown [3], this finite element result is interpreted as a steady state solution, although the remote plastic strain is

only of the order of the yield strain, and gives

$$\sigma_{rr\,\max} = 0.87\sigma_0.$$

In order to incorporate strain hardening in an approximate manner, the initial yield stress σ_0 was replaced by the current remote flow stress $\bar{\sigma}_\infty$ leading to

$$\sigma_{rr\,\max} = 0.87\bar{\sigma}_\infty.$$

Following McClintock and Rhee [6], strain hardening materials were viewed as being intermediate between non-hardening and purely elastic materials. Interpolation between the stress concentration resulting from the finite element analysis and Goodier's [2] analytic elastic solution gave

$$\sigma_{rr\,\max} = \bar{\sigma}_\infty$$

which was taken to represent the approximate behaviour of strain hardening materials. For triaxial stress states the remote mean stress $\sigma_{m\infty}$ is added to give the simple result

$$\sigma_{rr\,\max} = \bar{\sigma}_\infty + \sigma_{m\infty}.$$

4. Numerical analysis

In the present work, the problem of a spherical inclusion in a matrix subject to large remote plastic strains has been analysed using the MARC finite element program as modified by Rice and Tracey [7]. The program has a finite strain capability based on the analysis of McMeeking and Rice [8] with the stress and strain fields determined incrementally using the variational principle of Nagtegaal, Parks and Rice [9] applied over a mesh of isoparametric quadrilateral elements. Classical non-dilating constitutive relations were used for the inclusion analyses although it is possible from the work of Parks (unpublished) to specify dilating elements which behave according to the constitutive law associated with the Gurson [10] yield surface and hence to model the dilation of a porous aggregate material. The elements may be linear-elastic/perfectly plastic, linear-elastic/power-hardening or piecewise-linear and the program allows both axisymmetric and plane strain solutions to be obtained.

5. Analysis of a spherical inclusion

As the inclusion is symmetric, only the first quadrant of the complete problem need be modelled, as in Fig. 3, where the origin of the coordinate system is the centre of the inclusion. The finite element mesh was generated automatically using a procedure developed by Zienkeiwicz and Phillips [11] and is made up of 160 quadrilateral elements bounded by generators extending radially from the origin and by concentric circles. The origin is common to the 10 quadrilateral elements in the innermost ring which therefore appear as triangles. Smaller elements were specified towards the origin while larger elements were considered adequate for the remote boundaries. The inclusion comprises the 50 elements in the 5 rings nearest the origin while the remaining elements represent the matrix. This gives a remote boundary at approximately 6 times the inclusion radius. Symmetry implies that nodes on the y-axis ($x = 0$) should be constrained such that no displacement occurs in the x-direction and nodes on the x-axis ($y = 0$) should be constrained such that no displacement occurs in the y-direction. The boundary conditions at the inclusion-matrix interface depend on the assumed constitutive response of the inclusion.

It is not practicable to describe the behaviour of real materials in finite element terms without some simplification of inclusion and matrix response. This may take the form of

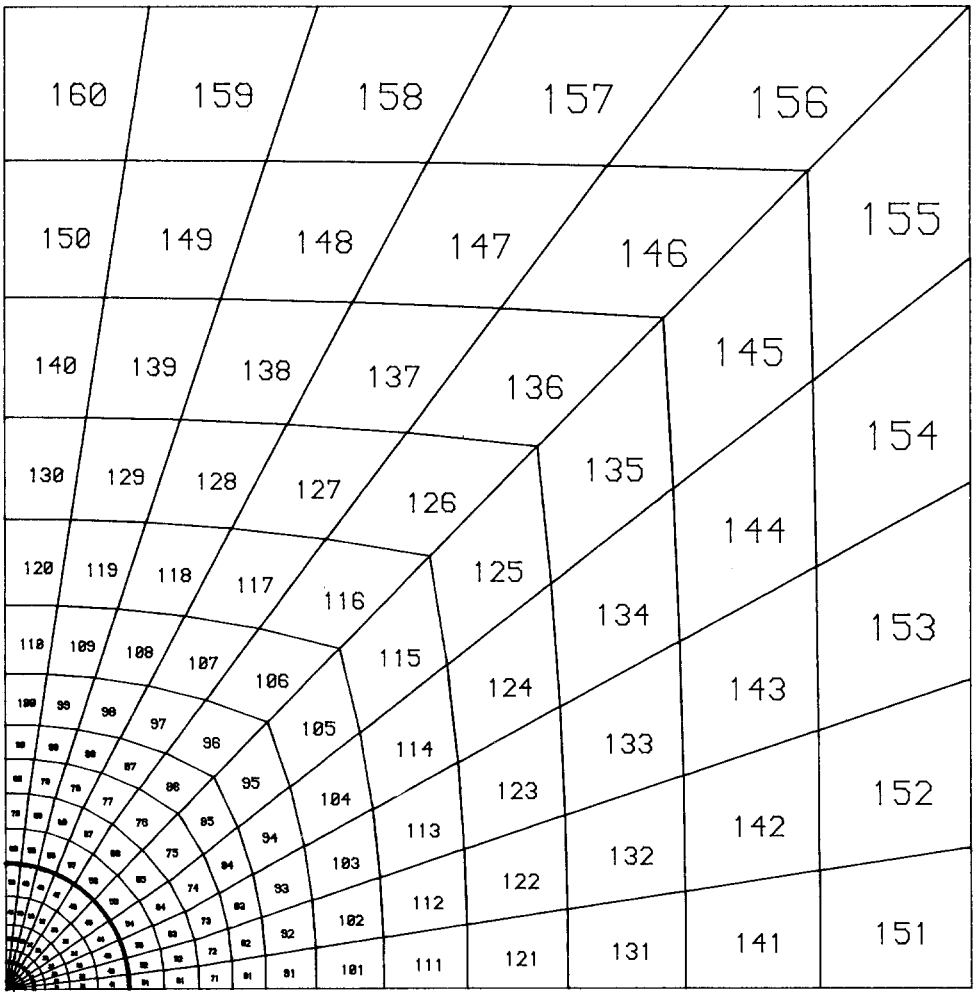

Figure 3. Finite element grid.

allowing only elastic deformation of the inclusion or indeed of considering the inclusion to be rigid. A rigid inclusion was simulated by constraining the nodes along the inclusion-matrix interface to have zero displacement in both the x and y directions. Such a model allows analysis of the matrix flow field but gives identically zero stress and strain fields within the inclusion. The model cannot therefore give any information about the interior of a real inclusion or of any internal stress or strain gradients.

A number of solutions have been obtained using different combinations of inclusion and matrix response. For comparison with the existing solutions, it is instructive to consider a rigid inclusion in a rigid/perfectly-plastic matrix. This cannot be modelled exactly using the available finite element program but the response of such a material is approximated by considering the matrix to have a high but finite elastic modulus. The effect of the elasticity of the matrix may be illustrated by a similar analysis of a rigid inclusion in an elastic/perfectly plastic matrix with an elastic modulus typical of structural steels. The role of matrix strain hardening may then be inferred from an analysis of a rigid inclusion in an elastic/power-hardening matrix. These solutions are presented in the following sections, the most general case being discussed first. In this, a power law

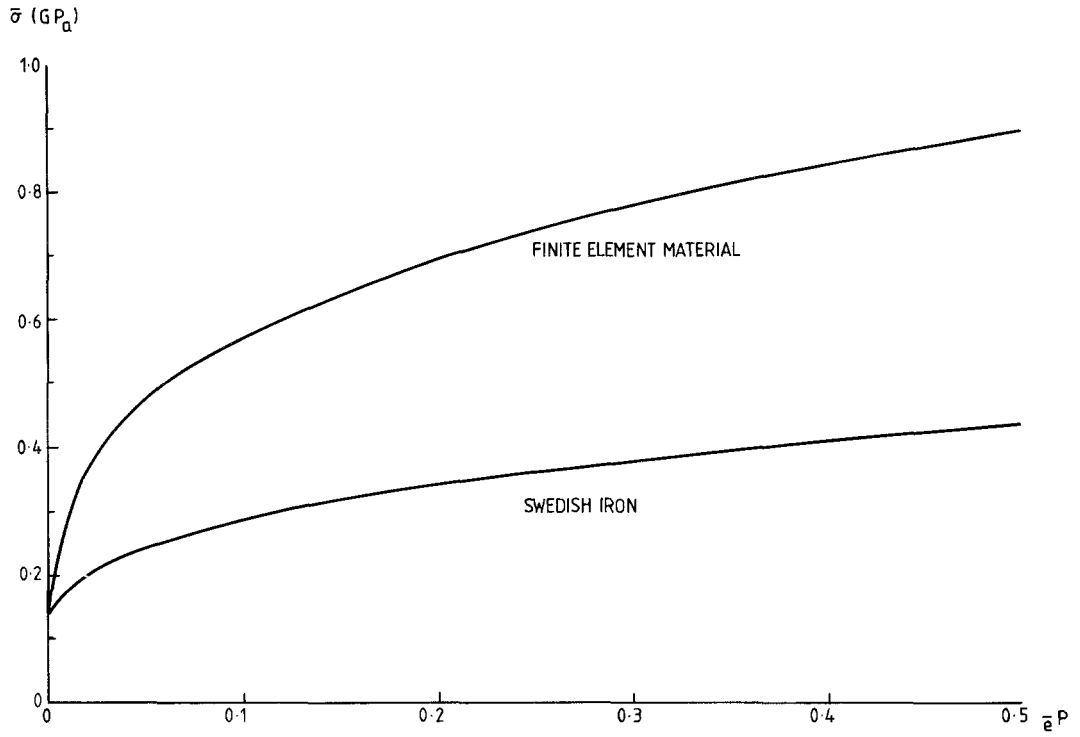

Figure 4. Power law stress-strain curves.

stress-strain curve of the form

$$(\bar{\sigma}/\sigma_0)^{(1/n)} - (\bar{\sigma}/\sigma_0) = (\bar{e}^p/e_0)$$

where

$$e_0 = \sigma_0/E$$

was used for the matrix although such an expression has a limited ability to describe the stress-strain relationship of real materials. An elastic modulus (E) of 210.0 GPa, an initial remote yield stress (σ_0) in uniaxial tension of 0.14 GPa and a power hardening index (n) of 0.28 were chosen to give a constitutive response (Fig. 4) representative of a low yield, strongly strain hardening material. In cases where it is necessary to model a specific material, a piecewise linear relation is more appropriate and such a relation was used for the analysis of the Swedish iron used in associated experimental work by Thomson and Hancock [12].

6. Results

6.1. Rigid inclusion in an elastic, power hardening matrix

The finite element model was subjected to 53 increments of displacement controlled uniaxial tensile loading along the remote boundary parallel to the x-axis, reaching a final remote plastic strain of approximately 15% or 220 times the initial yield strain. The finite element results typically showed the greatest stresses and strains in elements near the interface while contour plots of field variables such as the local flow stress $\bar{\sigma}$ (Fig. 5) and the local effective plastic strain $\bar{e}^p$ showed very small stress and strain gradients in the remote boundary elements. Significant gradients only developed near the inclusion-matrix

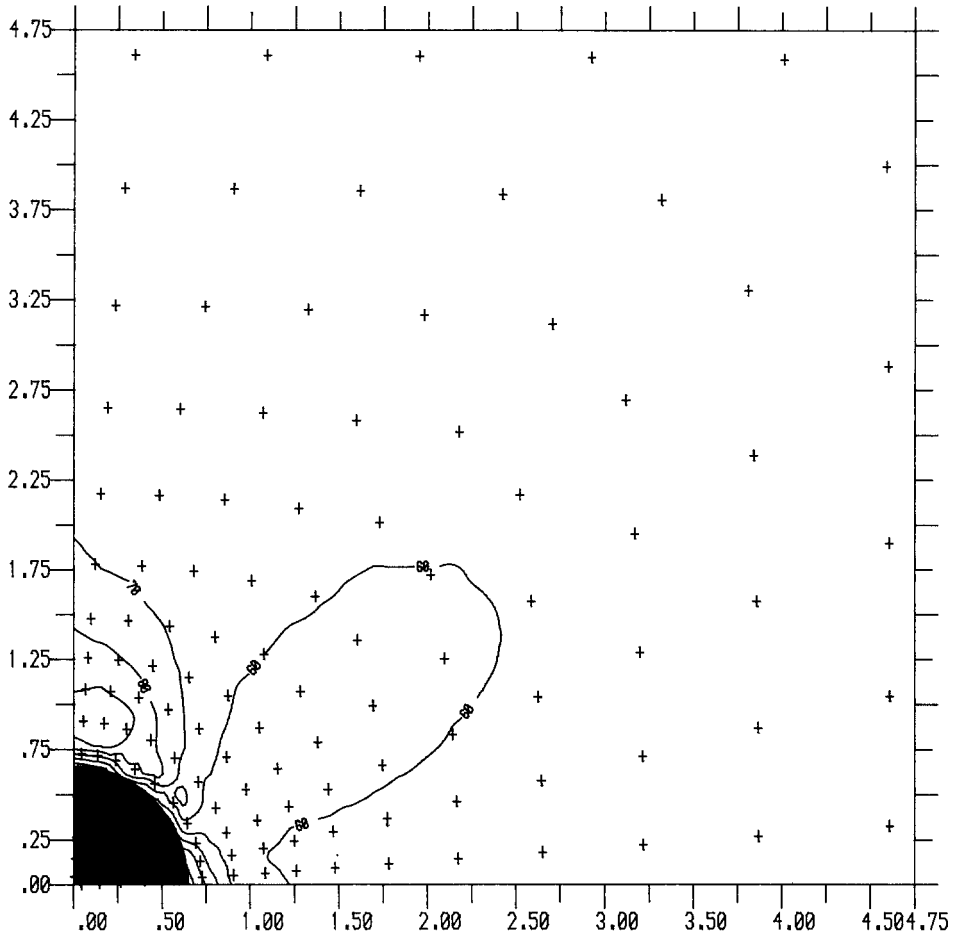

Figure 5. Flow stress remote from a rigid inclusion in a plastically deforming power-hardening matrix (+ denotes element centroid: $\bar{\sigma} = 0.6\sigma_0$ at contour 60).

interface (Fig. 6) which justified the representation of an isolated inclusion in an infinite matrix by a remote boundary at 6 times the inclusion radius. Contour plots can give a useful appreciation of the variation of quantities throughout the field of the analysis but some care is required in interpreting the region near the inclusion-matrix interface. Finite element solutions give values for field variables only at the centroids of elements and in this case the contouring routines which interpolate between these centroidal values attempt to draw some contours within the inclusion itself (Fig. 6), although the prescribed boundary conditions imply that field variables should be identically zero inside the interface. A finer mesh would reduce the spread of contours at the interface but the difficulty exists in principle for any grade of mesh.

Yielding first occurred above the pole of the inclusion but at a small distance from it, rather than at the interface itself. The resulting plastic zone spread with each increment of remotely applied load (Fig. 7) but the polar interfacial element did not yield until some time after its neighbours. This plastic zone extended to leave an elastic lobe at about 60° to the loading direction before full plasticity was finally reached. No large plastic strain concentrations were found on the interface while at large remote plastic strains the maximum plastic strain over the whole field was found to occur above the pole of the inclusion, a small distance from the interface. The maximum plastic strain on the interface developed at approximately $\pi/4$ to the loading direction, as shown by the contours in Fig.

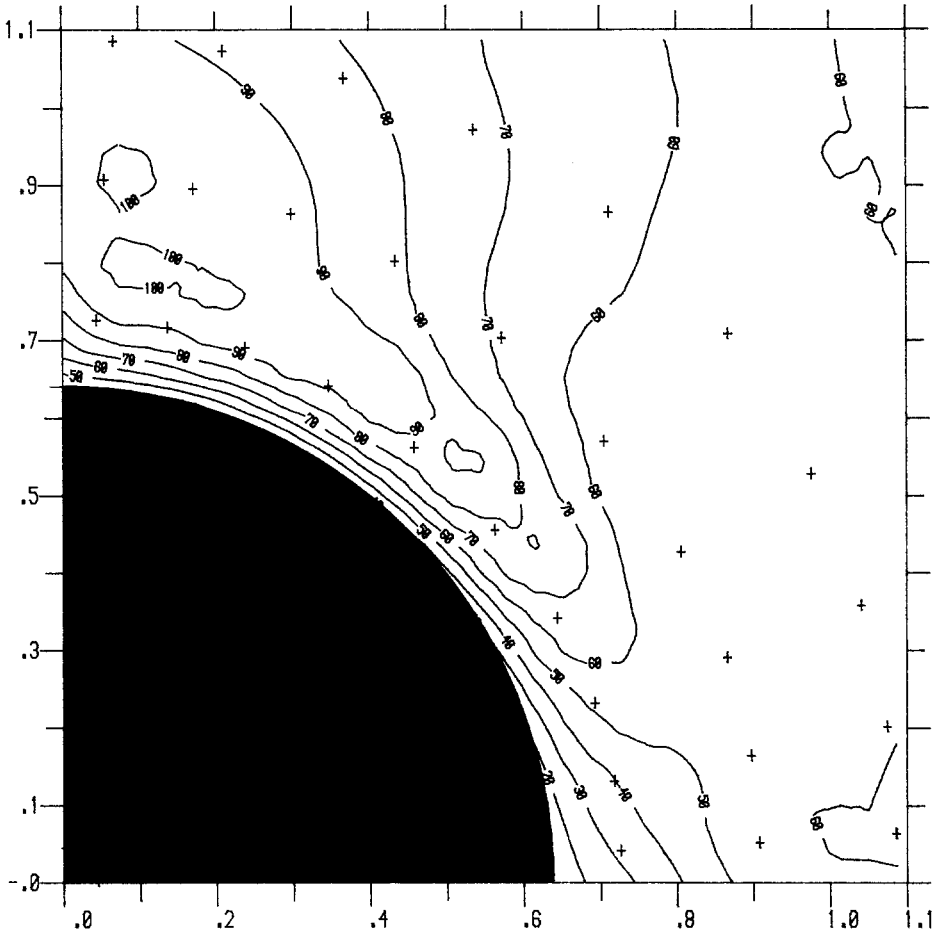

Figure 6. Flow stress near the interface of a rigid inclusion in a plastically deforming power-hardening matrix ($\bar{\sigma} = 0.6\sigma_0$ at contour 60).

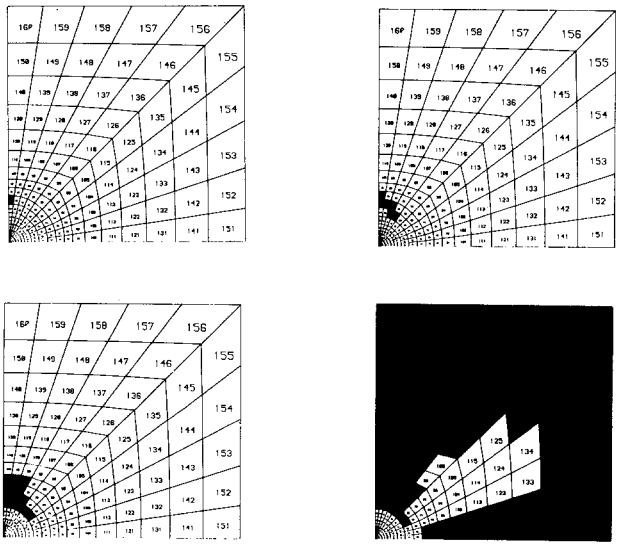

Figure 7. Development of the plastic zone around a rigid inclusion in a plastically deforming power-hardening matrix.

8. Figure 9 compares the local effective plastic strain ($\bar{e}^p$) in a number of significant elements. Since the remote elements were initially elastic, ordinates were plotted against the total remote strain component ($e_{yy\infty}$) in the loading direction, normalised with respect to the remote initial yield strain (e_0) in uniaxial tension. From Fig. 9 it is apparent that the plastic strain became progressively smaller as the pole of the inclusion was approached through the elements directly above it. These moderate interfacial strain concentrations became almost constant at large remote plastic strains, tending, for example, to approximately 1.1 at about $\pi/4$ to the loading direction and 0.8 in the polar element. The maximum interfacial effective stress coincides with the maximum interfacial effective plastic strain at approximately $\pi/4$ to the loading direction. In contrast, the maximum interfacial normal or radial stress $\sigma_{rr\max}$, calculated by transforming the stress components, was found to develop initially at the pole of the inclusion as shown in Fig. 10. As the deformation continued, the greatest interfacial radial stress moves away from the pole as shown in Fig. 11 which is also a feature of the work of Orr and Brown [3] and Argon, Im and Safoglu [4]. Figure 12 shows the maximum radial interfacial stress $\sigma_{rr\max}$ normalised with respect to the remote flow stress.

For strain hardening materials, the mean stress continues to rise with deformation but following an observation by Argon, Im and Safoglu [4] on the results of Orr and Brown

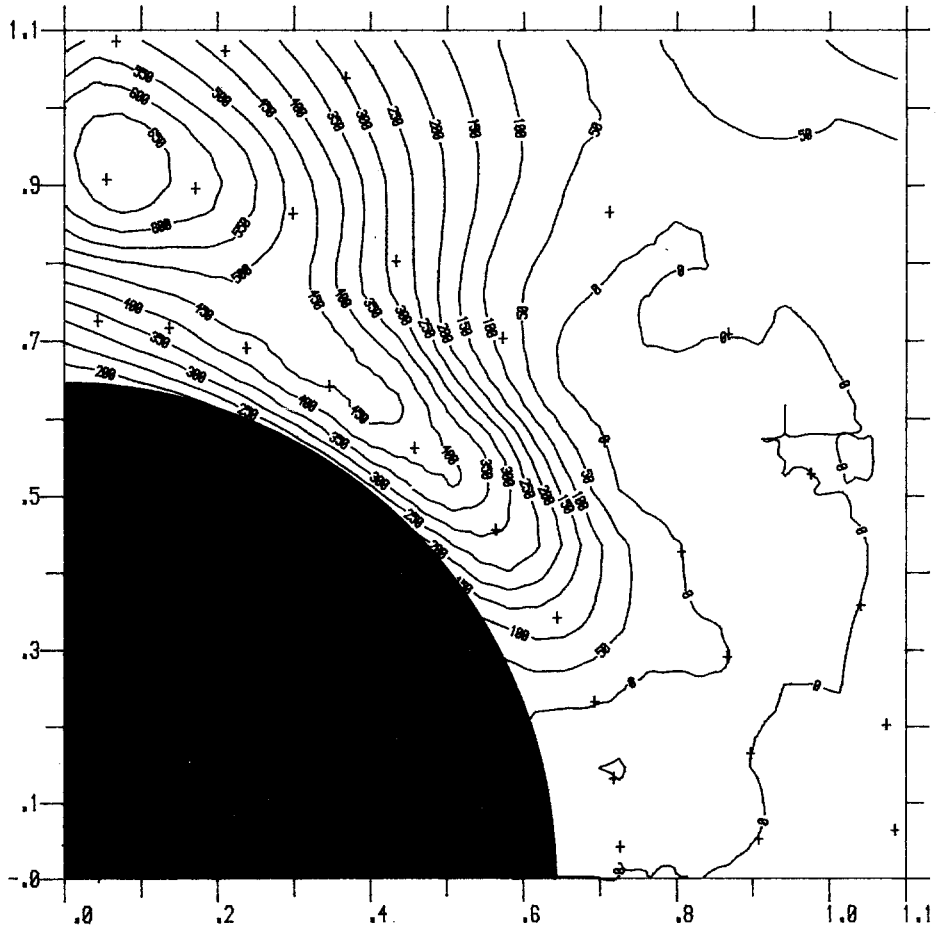

Figure 8. Effective plastic strain near the interface of a rigid inclusion in a plastically deforming power-hardening matrix ($\bar{e}^p = 0.5e_0$ at contour 500, $\bar{\sigma}_\infty = \sigma_0$).

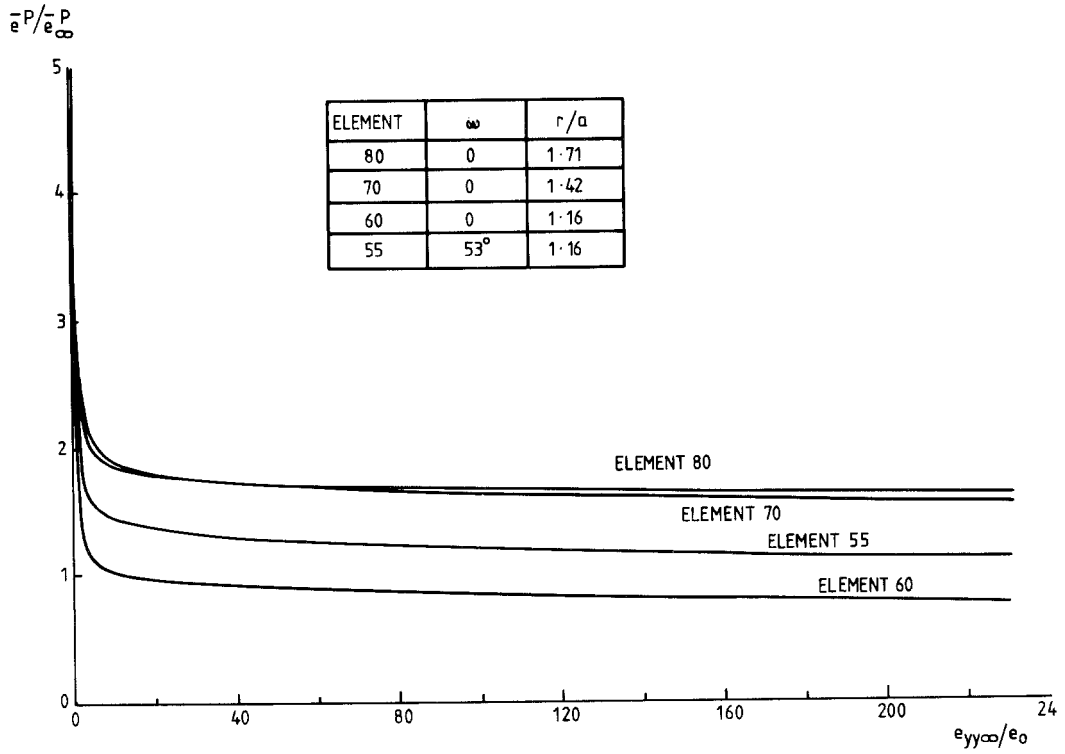

ELEMENT	ω	r/a
80	0	1·71
70	0	1·42
60	0	1·16
55	53°	1·16

Figure 9. Effective plastic strain in significant elements of a plastically deforming power-hardening matrix surrounding a rigid inclusion.

[3], the maximum interfacial radial stress was assumed to be of the form

$$\sigma_{rr\,\max} = C\bar{\sigma}_\infty + \sigma_{m\infty}$$

in which the appropriate remote mean stress $\sigma_{m\infty}$ is simply superimposed on the local interfacial stress field resulting from a purely deviatoric remote stress state of magnitude $\bar{\sigma}_\infty$. Figure 13 plots the value of C with increasing remote strain and shows that the interfacial radial stress concentration is not a constant, in contrast to the approximation of Argon, Im and Safoglu [4].

6.2. Rigid inclusion in an elastic, perfectly plastic matrix

A similar analysis was performed for a rigid inclusion in an elastic/perfectly plastic matrix with identical elastic constants to those used in the power hardening case ie $\sigma_0 = 0.14$ GPa and $E = 210$ GPa. The results of this large strain analysis of a non-hardening material showed similar trends to that of the power hardening analysis in the development of the plastic strain field (Fig. 14) and the stress fields (e.g. Fig. 15 for $\sigma_{rr\max}$). The development of the maximum interfacial radial stress (Fig. 16) did not reach a steady state value within the prescribed deformation.

6.3. Rigid inclusion in a high modulus, perfectly plastic matrix

It is not possible to specify infinite elastic stiffness in the finite element program used but the behaviour of such a material may be inferred from that of an elastic/perfectly-plastic material with a high elastic modulus. A finite element analysis was therefore performed

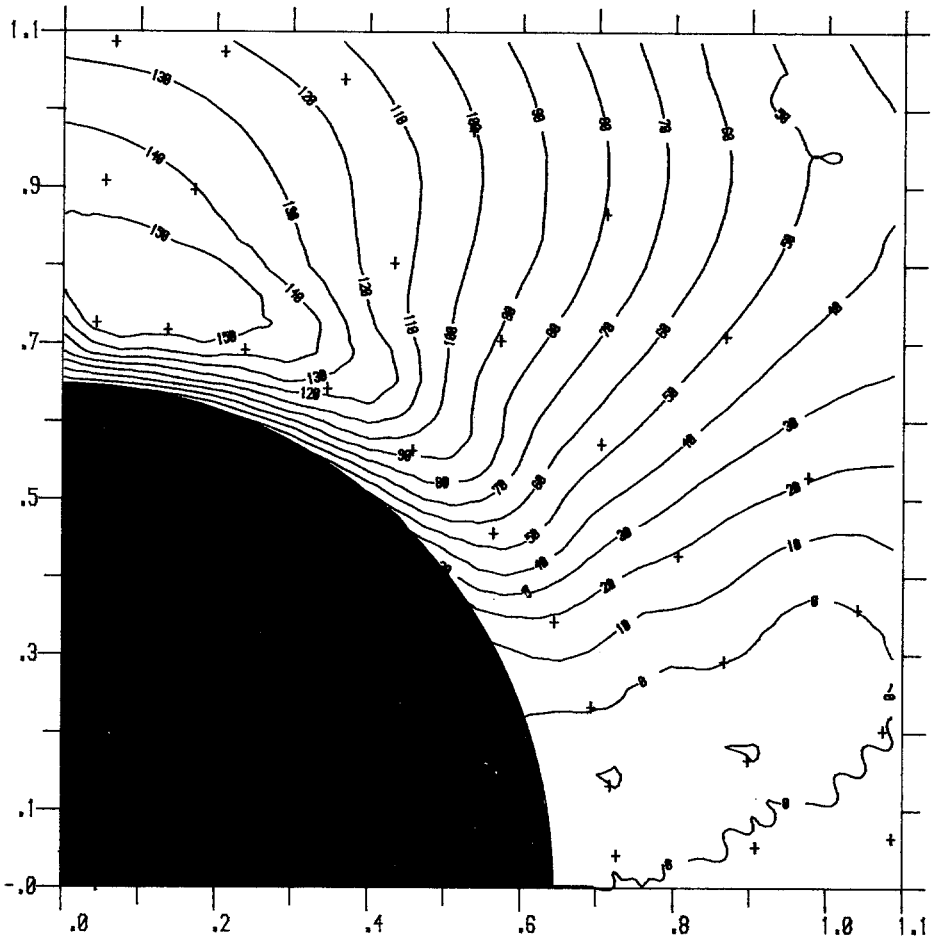

Figure 10. Stress component in a radial direction from the centre of a rigid inclusion for small remote effective plastic strains ($\sigma_{rr} = 1.4\sigma_0$ at contour 140, $\bar{\sigma}_\infty = \sigma_0$).

with a matrix of elastic modulus of 10^6 GPa. Increments of remote displacement loading were applied up to a total remote strain of 0.05% which though absolutely small, nevertheless corresponds to approximately 3500 times the initial yield strain. The trends of the results were similar to the previous analyses in that while the plastic strain concentration did appear to approach a constant value, no steady state occurred for the maximum interfacial radial stress.

The increase in the maximum interfacial radial stress was very rapid but can be conveniently shown by plotting the interfacial radial stress concentration against the remote effective plastic strain normalised with respect to the initial yield strain, $e_0 = 0.14/10^6$. With this scaling factor, the interfacial radial stress concentration is seen to develop in a manner which is remarkably similar to that for the elastic/perfectly-plastic material up to strains of the order of 80 times e_0 (Fig. 17), although the curves are very different when expressed as functions of absolute strain, which emphasises the importance of the elastic response of the matrix.

6.4. Oxide inclusion in an iron matrix

Swedish iron is a metallurgically simple material containing a single population of large iron oxide inclusions. The nature of the inclusion/matrix interface in this material is of

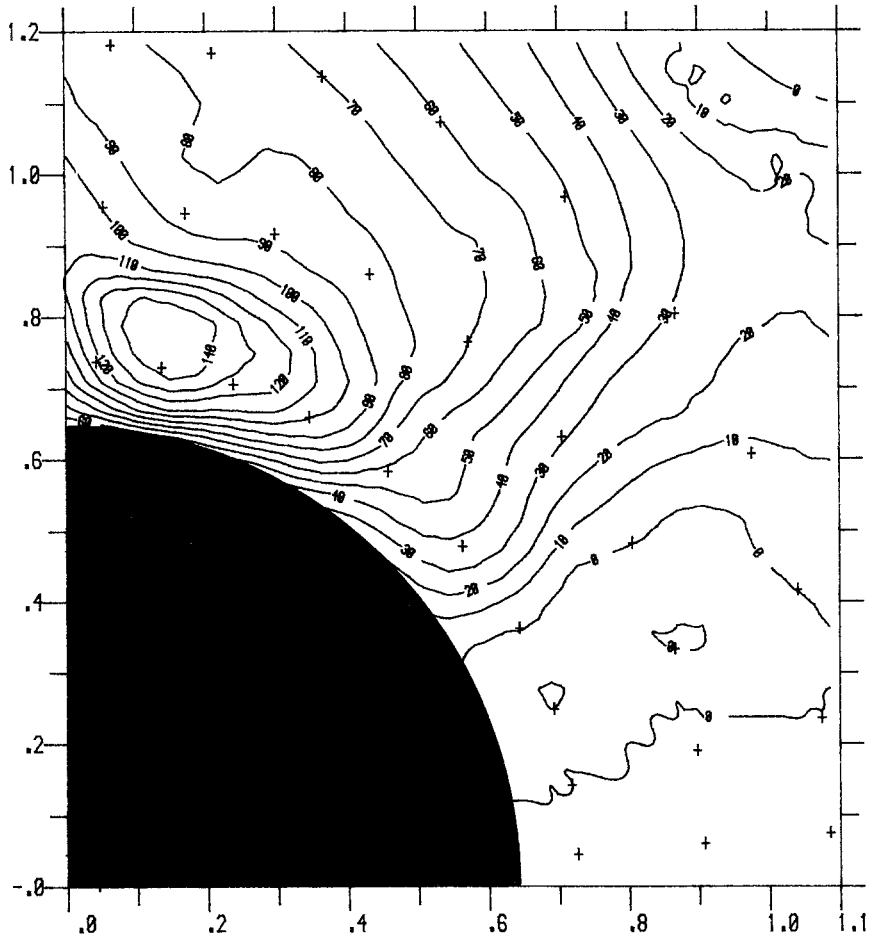

Figure 11. Stress component in a radial direction from the centre of a rigid inclusion for large remote effective plastic strains ($\sigma_{rr} = 14\sigma_0$ at contour 140, $\bar{\sigma}_\infty = 4.8\sigma_0$).

direct relevance to experimental work by Thomson and Hancock [12] and has been investigated by a finite element analysis of an elastic inclusion in an elastic/strain-hardening matrix, since the elastic constants of iron and the only oxide for which figures were available (Fe_3O_4) are of the same order [13].

Deformation of the inclusion was permitted by removing the displacement boundary conditions around the interface and extending the existing constraints along the coordinate axes to include the nodes within the inclusion itself. The specification of a high yield stress for the inclusion elements ensured that the deformation of the inclusion was purely elastic. For the analysis of this real material it was considered advisable to avoid the limitations of a power law through the use of a piecewise-linear approximation to the stress-strain equations of Swedish iron. The subsequent finite element analysis was found to be numerically stable up to very large plastic strain and remote displacements were applied to give a final absolute remote strain of 47% or 700 times the initial yield strain. This range was sufficient to cover the expected limits of void nucleation. Stress and strain gradients developed progressively within the inclusion itself with the maximum values of $\bar{\sigma}$ and of e_{yy}^{el} occurring near the interface at approximately $\pi/4$ to the axes and minimum values in the central elements. Graphs of the effective stress and elastic strain component in these elements (Fig. 18 and Fig. 19) show this progressive development but indicate that

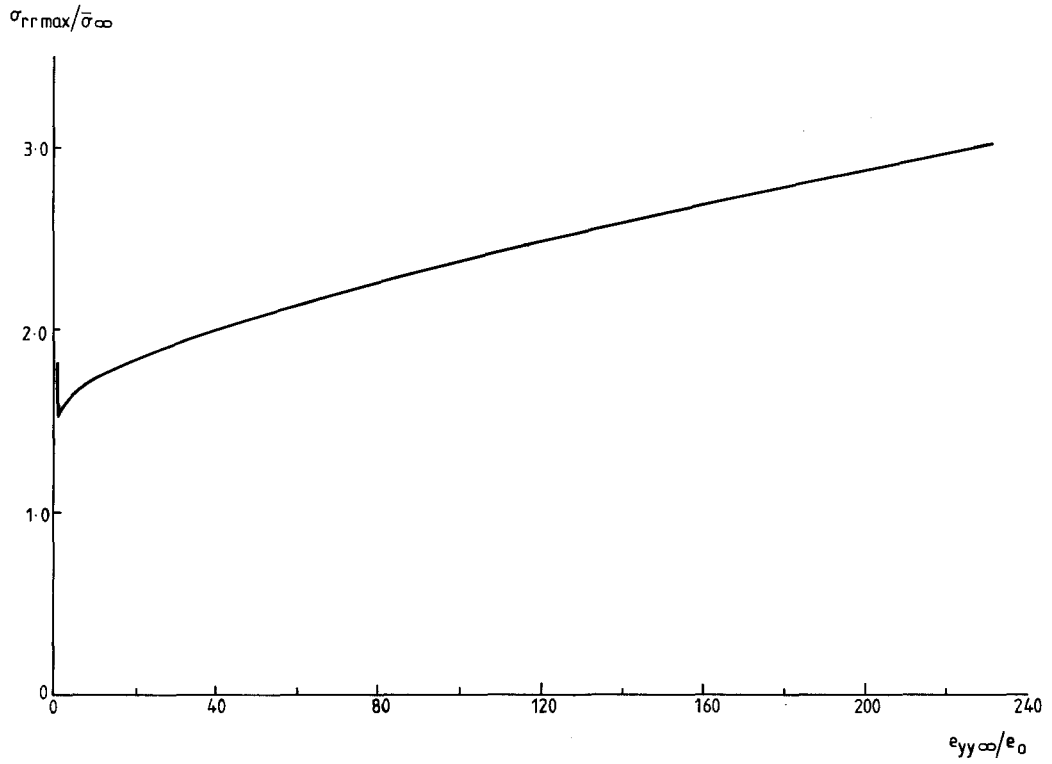

Figure 12. Maximum interfacial radial stress around a rigid inclusion in a power-hardening matrix.

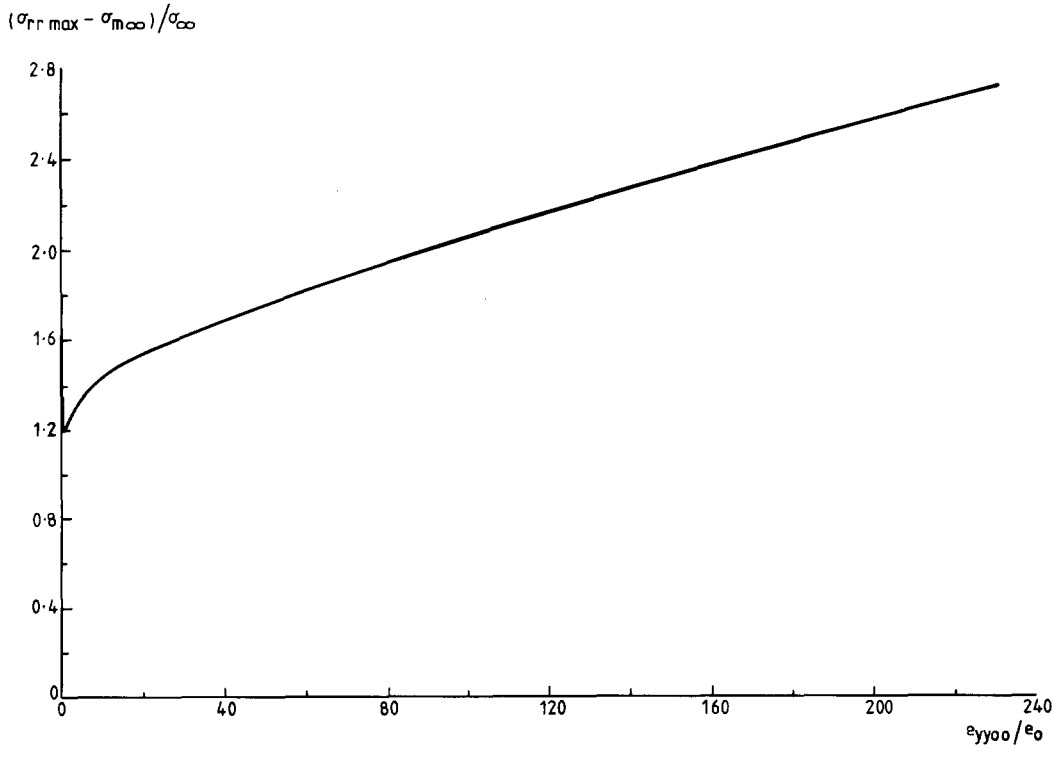

Figure 13. Maximum interfacial radial stress concentration around a rigid inclusion in a power-hardening matrix.

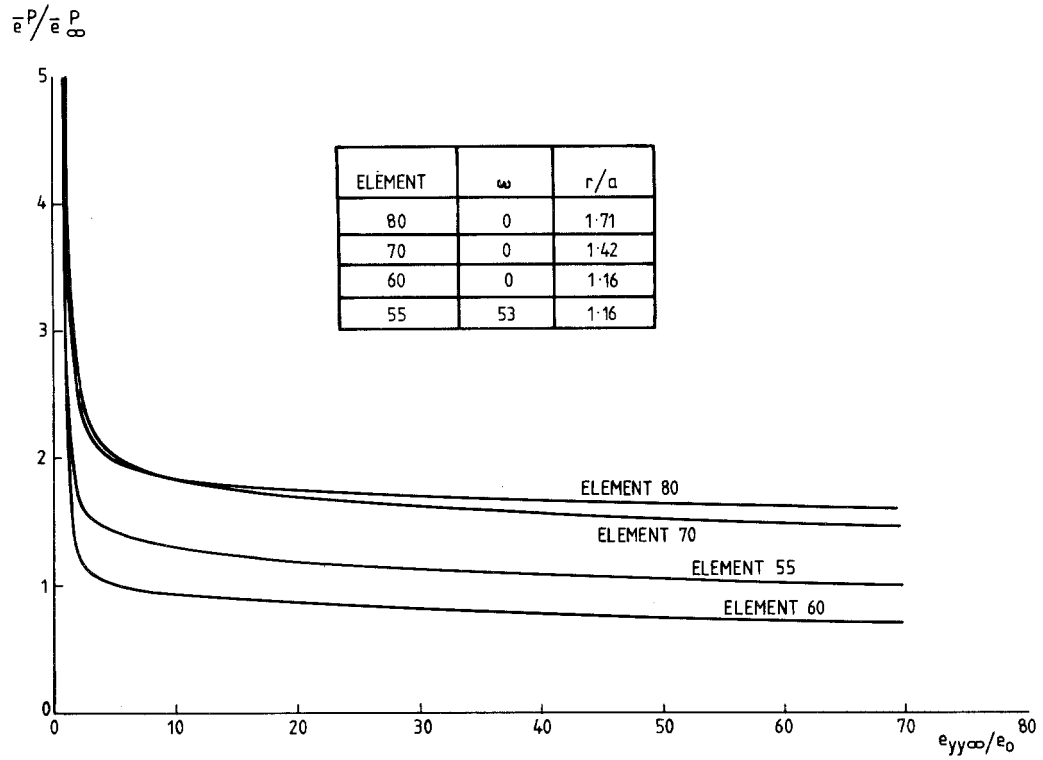

Figure 14. Effective plastic strain in significant elements around a rigid inclusion in a non-hardening matrix.

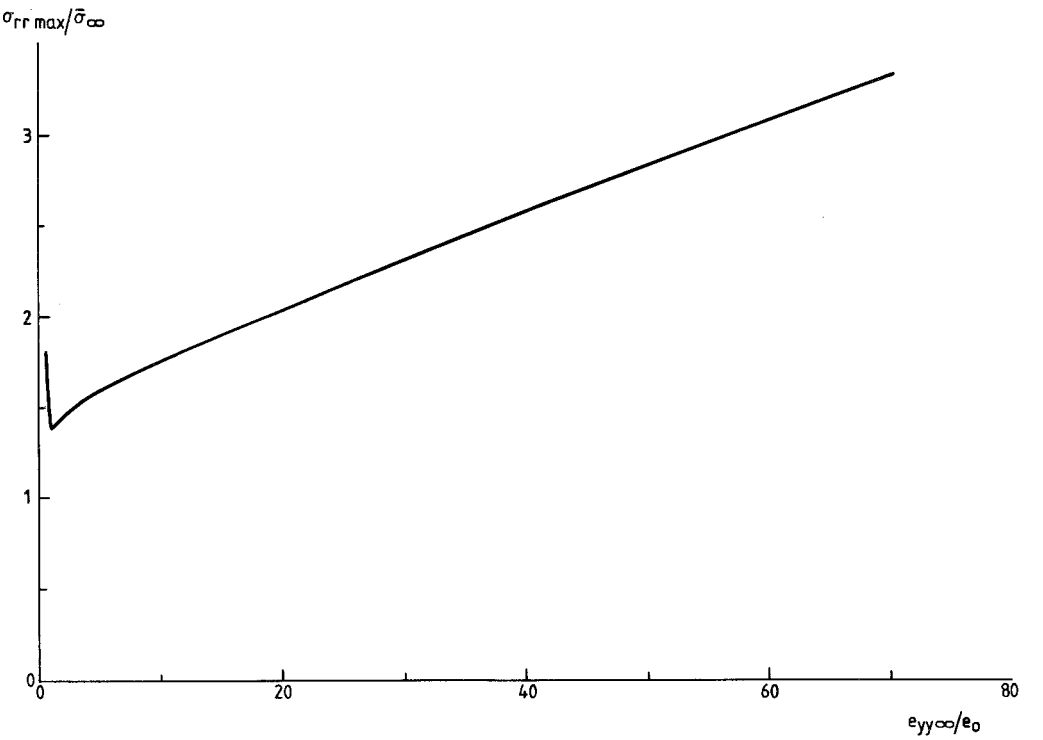

Figure 15. Maximum interfacial radial stress around a rigid inclusion in a non-hardening matrix.

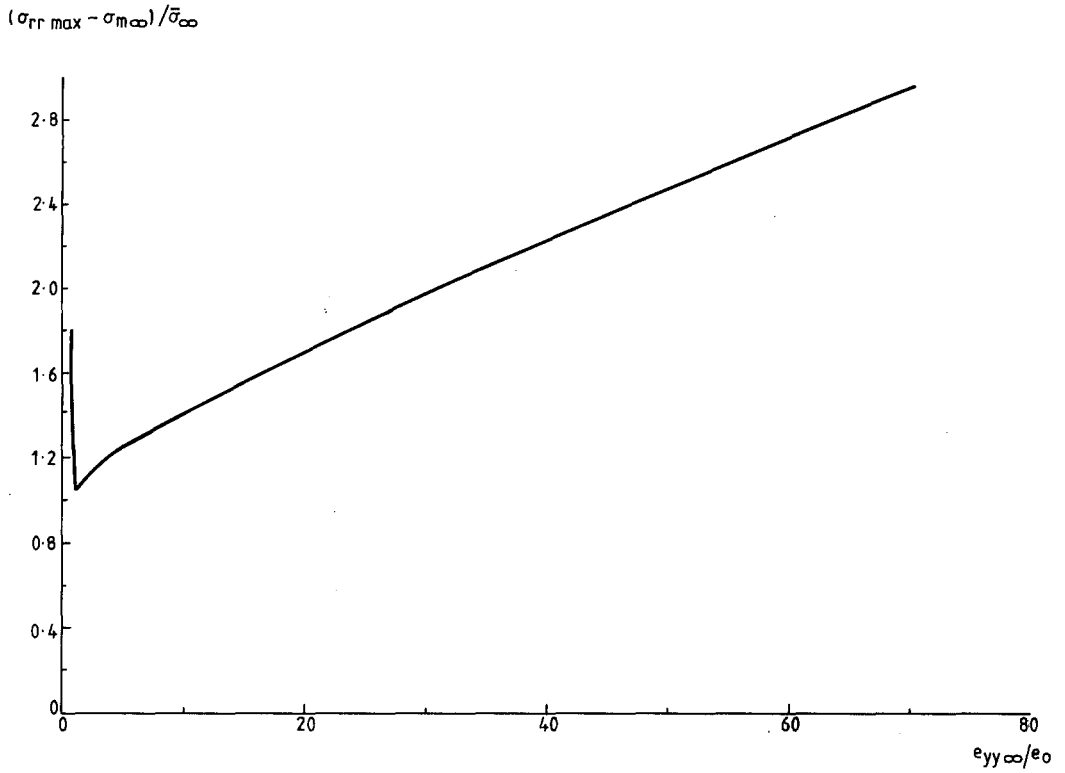

Figure 16. Maximum interfacial radial stress concentration around a rigid inclusion in an elastic, perfectly-plastic matrix.

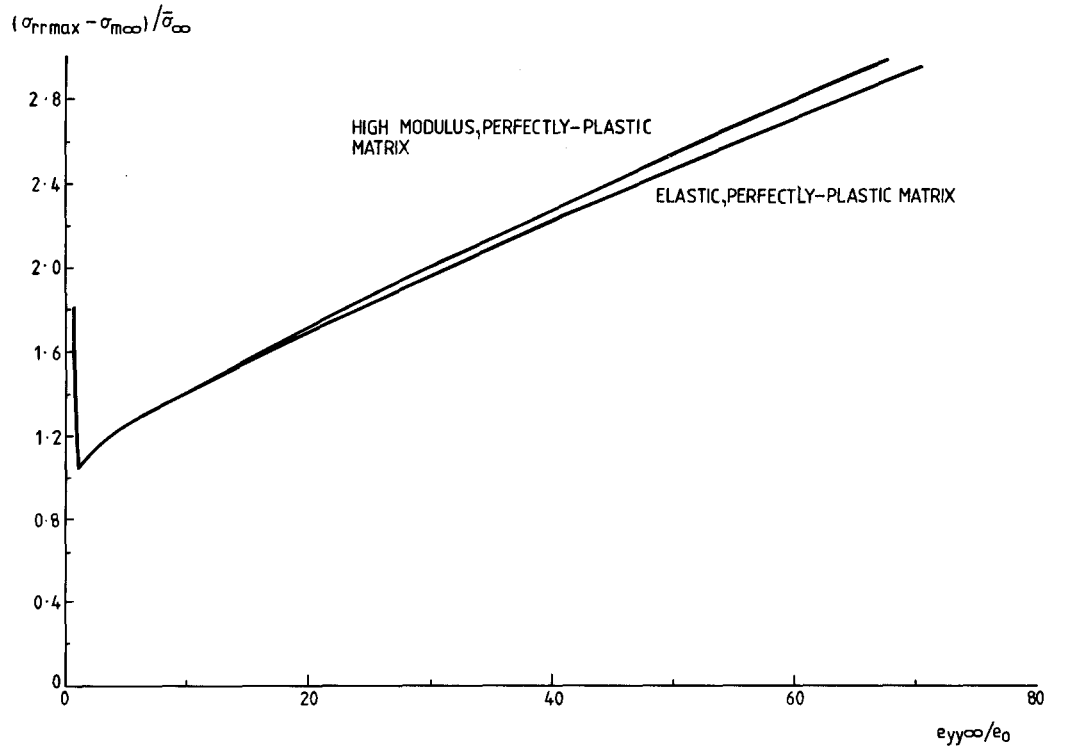

Figure 17. Maximum interfacial radial stress around a rigid inclusion in perfectly-plastic matrices.

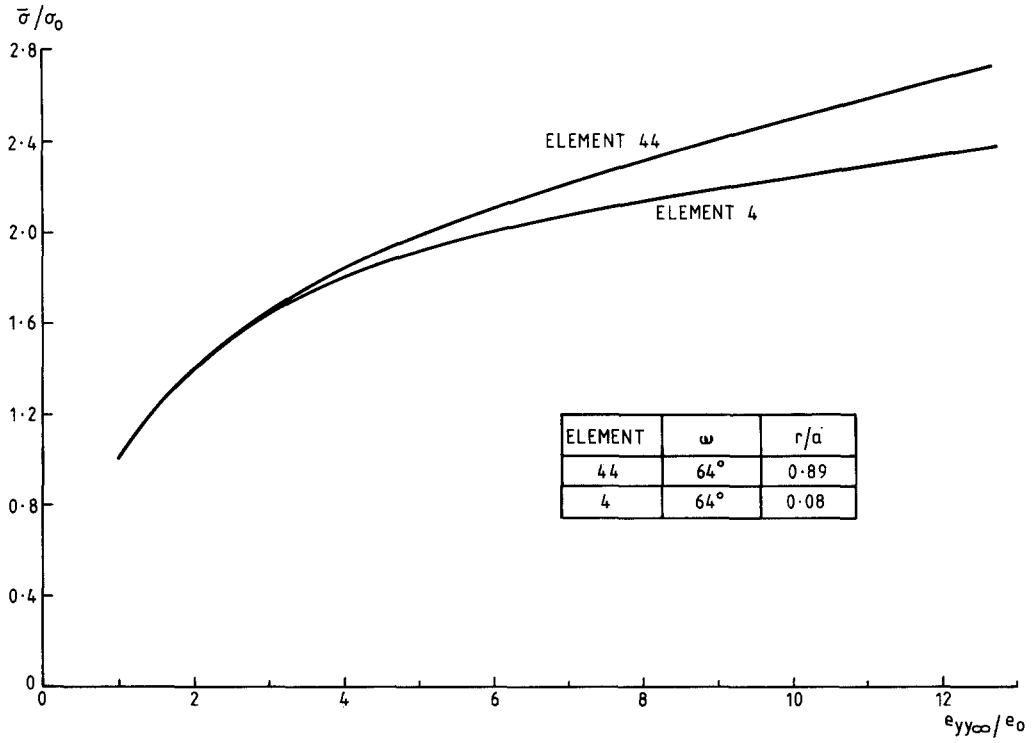

Figure 18. Development of effective stress gradient within an inclusion in a Swedish iron matrix.

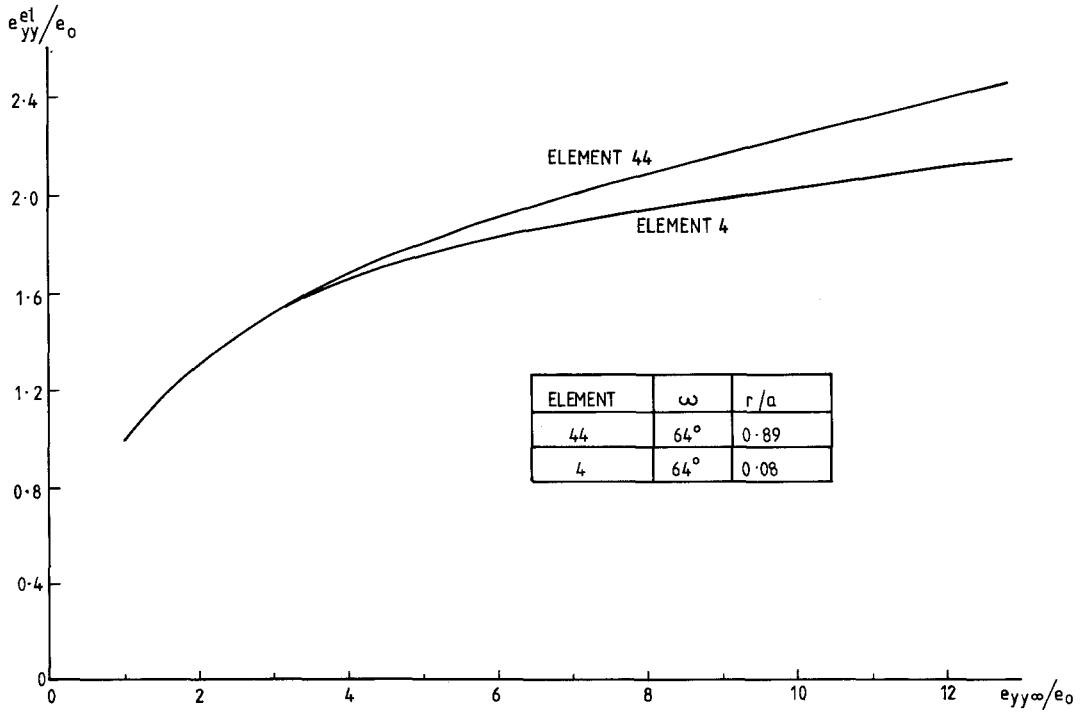

Figure 19. Development of elastic strain gradient within an inclusion in a Swedish iron matrix.

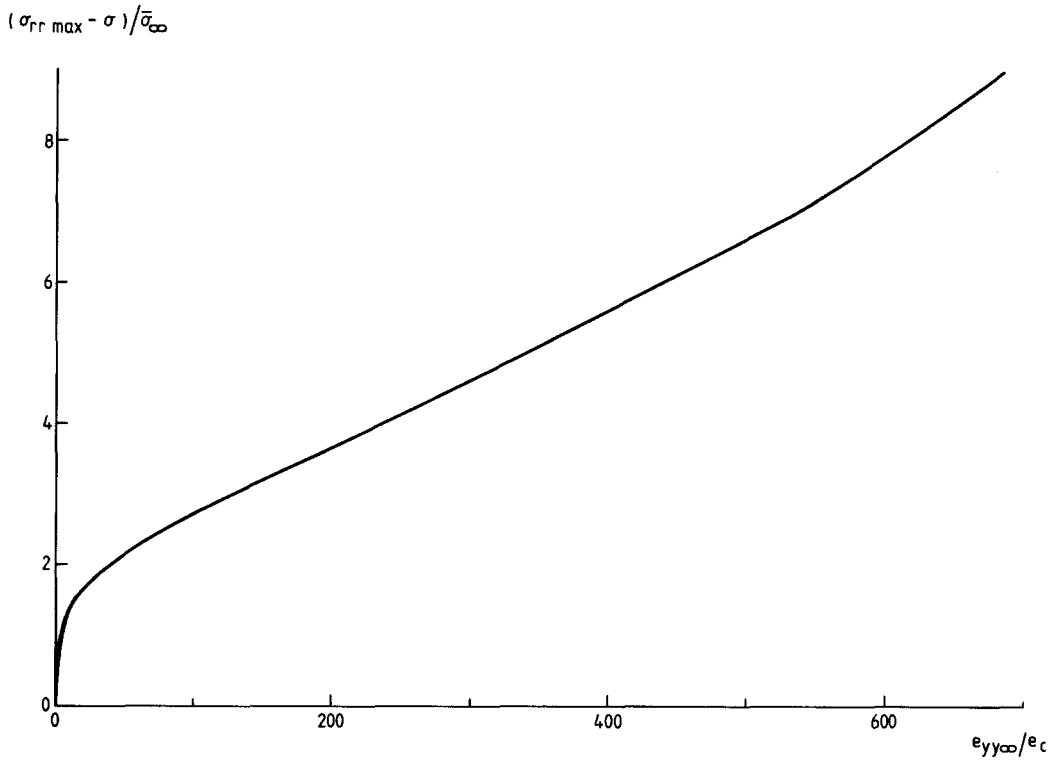

Figure 20. Maximum interfacial radial stress concentration around an elastic inclusion in a Swedish iron matrix.

the elastic deformation of the inclusion is homogeneous up to remote strains of the order of 10 times the matrix yield strain. Again the radial stress concentration on the interface does not reach a steady state (Fig. 20). No simple analytic expression was found to relate maximum interfacial radial stress to the remote loading but for specific materials subjected to finite strains it is perfectly adequate to express the variation of maximum radial stress in a piecewise analytic form. In the case of Swedish iron, the simplest expression which gave a reasonable description of the interfacial radial stress concentration was found to comprise a quadratic segment and two linear segments such that

$$C = -3.89.10^{-4}(\bar{e}^p_\infty/e_0)^2 + 4.83.10^{-2}(\bar{e}^p_\infty/e_0) + 0.8 \qquad 0 < (\bar{e}^p_\infty/e_0) < 60$$

$$C = 9.79.10^{-3}((\bar{e}^p_\infty/e_0) - 60) + 2.3 \qquad 60 < (\bar{e}^p_\infty/e_0) < 530$$

$$C = 1.40.10^{-2}((\bar{e}^p_\infty/e_0) - 530) + 6.9 \qquad 530 < (\bar{e}^p_\infty/e_0).$$

7. Discussion

The study of the stress and strain fields around an elastic inclusion in a plastically deforming matrix is motivated towards the determination of the local conditions which lead to failure of the interface. Initially it is instructive to examine the conditions at the pole of an inclusion where the symmetry conditions require that the interfacial shear strain be zero. For the rigid inclusion, compatibility demands that the total matrix hoop strains $e_{\theta\theta}$ and $e_{\phi\phi}$ are zero. These total strains however can have an elastic and plastic component such that,

$$e^{el}_{\theta\theta} + e^p_{\theta\theta} = 0.$$

Plastic flow at the pole is then only possible provided that plastic strains are balanced by equal and opposite elastic strains. In all the numerical analyses presented, the polar element has yielded but this may be a consequence of the finite dimensions of the mesh and it is not possible to say whether this would be a feature of an exact analytic solution. It must however be concluded that in the polar region the elastic strains cannot be neglected during plastic flow. In a steady state solution, the stress and strain concentrations are time independent provided geometry changes are insignificant. In a rigid/perfectly-plastic problem this steady state is usually reached soon after general yield and in finite-elastic/perfectly-plastic materials it is to be expected that steady state would be reached when the elastic strains become insignificant relative to the plastic strains. For the inclusion problem this condition is never reached at the pole as long as it continues to deform plastically. A steady state stress concentration may be attained in this location only if the polar material stops deforming and becomes rigid but this condition was not reached by any of the numerical solutions, including those by Argon, Im and Safoglu [4] and by Orr and Brown [3].

A common feature of all the elastic/plastic solutions is that the development of the plastic strain displaces the position of the maximum radial stress around the interface, away from the pole. This shift in the position of the maximum interfacial stress does not affect the validity of the argument for the pole but the existence of a shear strain may allow steady state to be reached earlier at this location. It is however clear that the proximity of the maximum interfacial stress to the pole means that the elastic strains are significant and the finite elastic response of the matrix inhibits the development of steady state to such an extent that interfacial failure in real materials is unlikely to occur in steady state conditions.

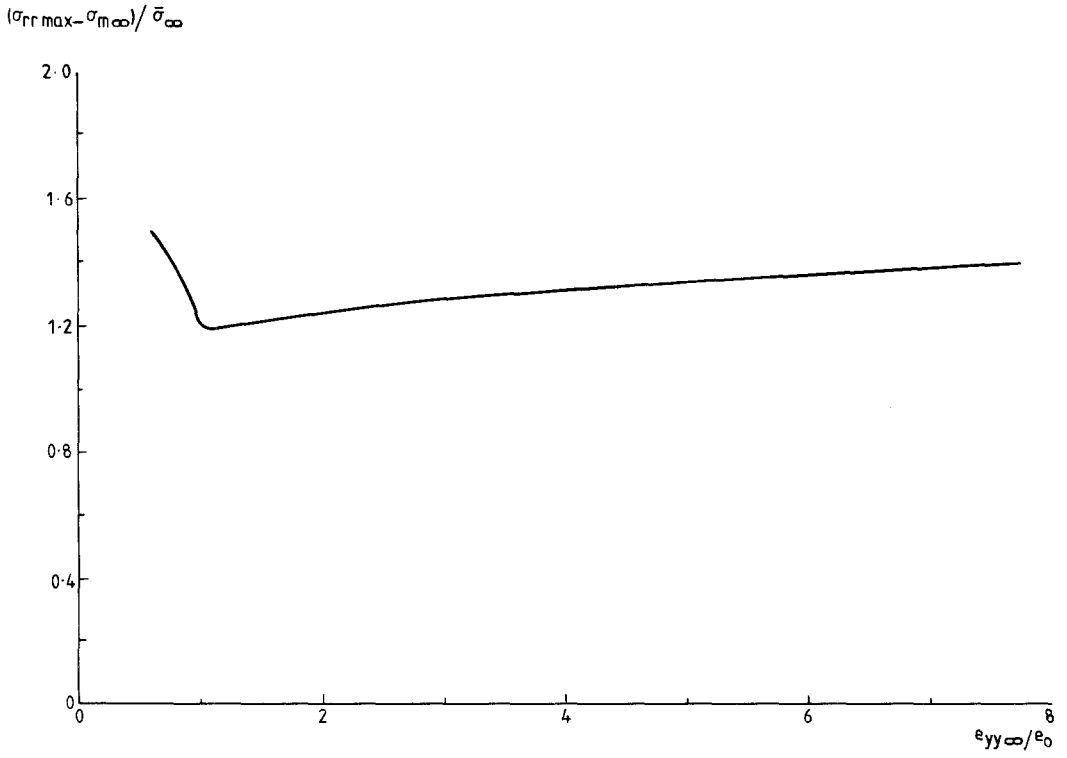

Figure 21. Maximum interfacial radial stress concentration around a rigid inclusion in a power-hardening matrix for small remote plastic strains.

In all the large strain solutions presented here the maximum interfacial radial stress continued to rise as the remote strain increased to more than two orders of magnitude times the initial yield strain, even for a non-hardening matrix. A similar conclusion was reached by Orr and Brown [3], in contrast to the conclusions of Argon, Im and Safoglu [4] whose analysis was however restricted to effective plastic strains of the order of the matrix yield strain. When the scale at the lower end of Fig. 13 was expanded to give Fig. 21, the value of the interfacial stress concentration was found to initially fall to a value of 1.2 at a remote strain of the order of the initial yield strain, in broad agreement with their results. As the loading continued, the interfacial stress concentration began to rise again and the apparent approach to a steady state is shown as the approach to a minimum turning point. This minimum turning point and the slow approach to a steady state in the development of the maximum interfacial radial stress are also features of the analyses of a hardening material. However, the data given allow estimates of the interfacial stresses and have been used by Thomson and Hancock [12] to determine the interfacial conditions leading to void nucleation at second-phase particles.

8. Acknowledgement

Acknowledgement is due to Dr. D.K. Brown and Dr. M.J. Cowling of the Department of Mechanical Engineering, University of Glasgow, for much helpful discussion. The work was carried out with the assistance of the SERC Marine Technology Program Grant in the Department of Mechanical Engineering at the University of Glasgow. Appreciation is expressed for the facilities afforded by the former Project Coordinator, Prof. J.D. Robson, and to Prof. B.F. Scott.

References

[1] J.D. Eshelby, *Proceedings of the Royal Society* A241 (1957) 376–396.
[2] J.N. Goodier, *ASME Applied Mechanics Magazine* 55 (1933) 39–44.
[3] J. Orr and D.K. Brown, *Engineering Fracture Mechanics* 6 (1974) 261–274.
[4] A.S. Argon, J. Im and R. Safoglu, *Metallurgical Transactions* 6A (1975) 825–837.
[5] P.V. Marcal and I.P. King, *International Journal of Mechanical Sciences* 9 (1967) 143–155.
[6] F.A. McClintock and S.S. Rhee, in *Proceedings of the 4th US National Congress on Applied Mechanics* 2 (1962) 1002.
[7] J.R. Rice and D.M. Tracey, *Journal of the Mechanics and Physics of Solids* 17 (1969) 201–217.
[8] R.M. McMeeking and J.R. Rice, *International Journal of Solids and Structures* 11 (1975) 601–616.
[9] J.C. Nagtegaal, D. Parks and J.R. Rice, *Computer Methods Applied Mechanical Engineering* 4 (1974) 153–177.
[10] A.L. Gurson, *Transactions ASME Journal of Engineering Materials Technology* 99 (1977) 2–15.
[11] O.C. Zienkiewicz and D.V. Phillips, *International Journal of Numerical Methods in Engineering* 3 (1971) 519–528.
[12] R.D. Thomson and J.W. Hancock, To be published (1984).
[13] *American Institute of Physics Handbook*, 3rd Ed, McGraw-Hill, New York (1972) 2–52.

Résumé

A une échelle microscopique, une rupture démarre souvent au voisinage d'inclusions dans une matrice déformée où les conditions de contrainte et de déformation locales peuvent conduire soit à une rupture de l'interface inclusion/matrice ou de la particule elle-même. Des solutions analytiques sont disponibles pour déterminer les champs locaux de contrainte et de déformation au voisinage d'une inclusion élastique dans une matrice élastiquement déformée, mais pour des déformations plastiques, il est nécessaire de recourir à des analyses numériques. On présente ici une solution numérique applicable à une inclusion élastique sphérique dans une matrice élasto-plastique, en se concentrant largement sur l'interface particule/matrice qui est en cause dans la rupture ductile. Des solutions sont également présentées pour des inclusions rigides et élastiques situées dans des matrices en matériau durcissable ou non durcissable.